

Investigation of CNT and Zn doped Cu-SSZ-13 zeolite catalyst for ammonia selective catalytic reduction activity of NO_x

M. Sunil Kumar*, M. S. Alphin

Department of Mechanical Engineering, Sri Sivasubramaniya Nadar College of Engineering, Kalavakkam, Chennai- 603110, India

Hybrid Cu-SSZ-13 zeolite catalyst are prepared and analyzed for NH₃-SCR activity with different topologies in the present investigation. Cu-SSZ-13 was synthesized by ion-exchange method, and hybrid Cu-SSZ-13 was synthesized by wet-impregnation method with three different molar ratios between Zn_x-CNT_y as 1:5, 1:10, & 1:15 and maintained as 1:5 mass ratio between Zn_x-CNT_y/Cu-SSZ-13 hybrid zeolite catalysts. The catalytic activity measured at a temperature window of 100°C to 550°C concludes hybrid Zn₁-CNT₁₀/Cu-SSZ-13 catalyst exhibits high NH₃-SCR performance (100%) at a temperature of 180°C to 475°C and by anti-sulfur activity, it exhibits 80% NO_x at 300°C for 8hrs in the presence of SO₂ gas in feed aid that addition of Zn species and CNTs influence Cu-SSZ-13 in NH₃-SCR activity finding them to be a better catalyst for NO_x reduction.

(Received August 22, 2022; Accepted November 23, 2022)

Keywords: NH₃-SCR, Cu-SSZ-13 zeolite catalyst, Anti-sulfur activity, NO_x conversion, Carbon nano-particle, Wet impregnation

1. Introduction

NO_x emission became stringent to the environment from several and to comply with Euro VI emission standards, SCR is the most affluent technology [1]. Several advanced reserachers on doping metal oxides and ion exchange with zeolite to better the NH₃-SCR [2], [3] have been carried out recently. Emphasis on Cu-SSZ-13 zeolite catalysts was made as they exhibit optimized and excellent performance characteristics with high hydrothermal stability by replacing the commercial catalyst in NH₃-SCR catalyst [4], [5] though they suffer SO₂ poisoning [6]–[16]. Doping proved to be a better way to overcome this and in particular with the Zn which has the best regeneration capacity substantially controlling SO₂ poisoning at both lower and higher temperature regimes [17]–[20] and also its higher thermal stability providing better NH₃-SCR performance [1], [21].

Fewer recent reports on the deactivation mechanism of Cu-CHA catalyst was made and it is identified that as increasing Cu loading in zeolite catalysts, the number of sulfate species adsorbed will increases [22]. Hammershoi et al. suggested that there is a superficial relation existence between SO₂ and Cu species, while catalyst undergoes SO₂ exposure [15], [23] copper sulfate and ammonia sulfate act as active agents to poisoning the active site during low-temperature deactivation of NH₃-SCR reaction [10]–[15]. This formation of sulfate species is mainly due to two process parameters such as reaction temperature and composition of feed gas [10]–[12], [24]. More comparatively, H₂O forms a stable sulfate species than NH₃ presence forms ammonium sulfate species to a larger extent. Still, SO₃ formation will create a huge amount of deposition over support pores with significant deactivation [8], [12]–[20], [22], [25]. During high-temperature treatment, copper sulfate species possess high thermal stability and decompose at a temperature of 550°C which is irreversible [3], [13]. But at low temperatures, ammonium sulfate species are responsible for catalyst deactivation due to fierce adsorption between SO₂ and NO_x.

To consice, a hybrid catalyst is identified as the best solution to evade poor low and high temperature activites in NH₃-SCR activity. The present investigation aims to bring down the NO_x

* Corresponding author: sunil240697@gmail.com
<https://doi.org/10.15251/DJNB.2022.174.1313>

by preparing a hybrid catalyst with Cu ion-exchanged and metal doped with Cu-SSZ-13 zeolite catalyst and investigate its SO₂ endurance and NH₃-SCR activity. Influence of CNT doping is also explored under the same set of studies and thermo-physical property evaluation are made on the catalysts prepared with advanced characterization techniques being involved.

2. Catalyst preparation

The sodium form of conventional zeolite Na-SSZ-13 (Si/Al = 20) zeolite was purchased from ZR catalyst Pvt Ltd., China. Na-SSZ-13 was converted into Cu-SSZ-13 by treatment of ion exchange with 0.5 M of NH₄NO₃ to form NH₄-SSZ-13 at 80°C followed by 0.04 M of aqueous Cu(CH₃COO)₂ to form Cu-SSZ-13 at 40°C where cation substitution was taken to exchange NH₄ ion by Cu²⁺ ions. Zeolite slurry formed was kept in the oven to dry at 110°C after filtering the slurry and followed by washing with deionized water. Finally, samples were calcined at 550°C for 5hrs in a muffle furnace and samples are crushed and sieved to have the precursors for the hybrid catalyst of Cu-SSZ-13 and high purity (Purity > 98%) multiwall carbon nanotubes with length and diameter of 10µm and 10-15nm were purchased from Sigma Aldrich were directly used for catalyst preparation without undergoes any further treatment. The hybrid catalyst was prepared by the wet-impregnation method and zinc nitrate was used as a precursor for zinc (Zn).

Further, in wet impregnation, zinc nitrate and multiwall carbon nanotubes were dispersed in water and ethanol individually with the aid of ultrasonicator for 1.5h and Cu-SSZ-13 zeolite was added to the Sol ultrasonicated for 1h. The evolved solution was agitated (1h) and oven dried at 120°C, 2h. Dried powders were calcinated at 500°C, 5h followed by mechanical milling and sieving before proceeding for characterization. The final catalyst was mentioned as Zn_x-CNT_y/Cu-SSZ-13, where x and y represent a molar ratio of Zn and CNT varied from 1:5 to 1:15 and the mass ratio is maintained as 1:5 [1] between catalysts such as Zn-CNT and Cu-SSZ-13.

3. Catalyst characterisation

ASAP2020 physical absorbers were used to measure the Brunauer-Emmett-Teller (BET) surface area, pore diameter, and pore volume of the catalyst prepared by the wet impregnation method following X-ray diffraction analysis using EMPYREAN in the bragg's angle of 5° to 90° with CuKα (1.54Å) as majority of the search peas fall under this regime as per ICPDS database. SEM-EDS (Carl Zeiss EVO-18) morphological studies were made further along with identification of chemical states using XPS in support of the XRD results. The ammonia temperature-programmed desorption (NH₃-TPD) experiment was performed to analyze the ammonia storage capacity and acidity levels of the catalyst. Pre test preparation of samples (300 mg each) include exposing to helium for 1h, 200°C with a temperature gradient maintained at 10°C/min. Thereafter, at a flow rate of 30 mL/min, 10% of NH₃ was exposed until the catalyst was saturated by adsorption of NH₃. The unabsorbed NH₃ was removed with N₂ at a flow rate of 30 mL/min by purging the catalysts and results are recorded at 100°C and 750°C and SO₂-TPD experiment was carried out with same procedure of pre-treatment to remove carbon dioxide and water vapor and processing were carried out with 0.5% SO₂/He at a feed rate of 50 mL/min at a ramping rate of 10°C/min until temperature to reach 750°C.

4. Catalytic activity measurement

300 mg of catalyst were used to perform catalytic activity measurement in a fixed-bed stainless steel reactor (10 mm I.D) between the operating ranges of 100 to 550°C under 30,000h⁻¹ gas hourly space velocity. Fourier transform infrared spectrometer (VE FT-8000, Vasthi Instrument, India) and thermocouple were used to measure NO, N₂O, NO₂, and NH₃ concentration and temperature of the catalyst which is placed in the mid-portion of the reactor respectively. Fig.1

represents schematic diagram of experimental setup. 500 ppm NO, 500 ppm NH₃, 6% O₂, 200 ppm SO₂ (while used), 5% H₂O (while used), and remaining N₂. To introduce H₂O into the feed gas, a water bubble was used. The reaction temperature and total flow rate at which activity and model gases are introduced as 100 to 550°C and 500 mL/min. The conversion efficiency of NO_x and selectivity of N₂ for the prepared catalyst were calculated as follows [26], [27]:

$$\text{NO}_x \text{ conversion efficiency} = \frac{[\text{NO}]_{\text{Inlet}} - [\text{NO}]_{\text{Outlet}}}{[\text{NO}]_{\text{Inlet}}} \times 100 \quad (1)$$

$$\text{NH}_3 \text{ conversion efficiency} = \frac{[\text{NH}_3]_{\text{Inlet}} - [\text{NH}_3]_{\text{Outlet}}}{[\text{NH}_3]_{\text{Inlet}}} \times 100 \quad (2)$$

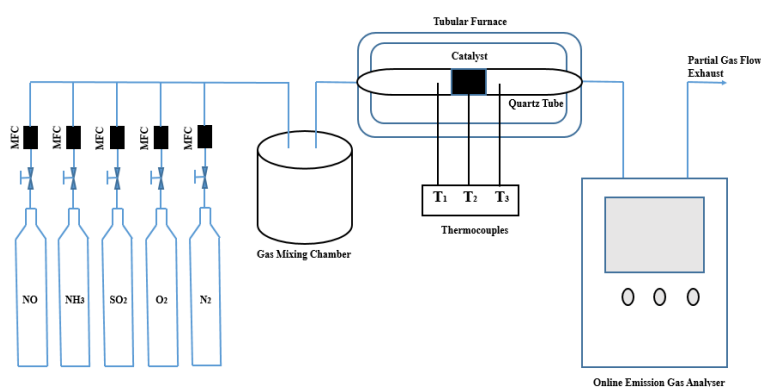


Fig. 1. Represents schematic diagram of experimental setup.

5. Results and discussion

5.1. Characterization

5.1.1 XRD Analysis

The XRD pattern of Cu-SSZ-13 and hybrid Cu-SSZ-13 zeolite catalyst as shown in Fig.2 exhibits the diffraction peaks at 9.5°, 14.0°, 16.1°, 17.8°, 20.7°, 25.0°, and 30.7° of crystalline nature attribute to the chabazite SSZ-13 zeolite structure [28]–[30]. As Zn species doping over Cu-SSZ-13 reduces their respective peak intensities means Zn species are well dispersed on the surface of Cu-SSZ-13 zeolite influences the surface area of it. With the introduction of CNT into Zn/Cu-SSZ-13, the surface area gets increased and CNTs are ascribed at 26.4° and 42.5° peaks, which were absent in Cu-SSZ-13 and Zn/Cu-SSZ-13 zeolite XRD fringes [31]. Also, a reduction in the peak intensity is observed with the CNT doping which attributes to the residual stress formation evident from the peak broadening. Also, it can be concluded that the Cu-SSZ-13 and hybrid Cu-SSZ-13 zeolite catalyst exhibits better crystalline structure without any impurities due to doping of Zn species and CNTs over Cu-SSZ-13 based on the XRD results.

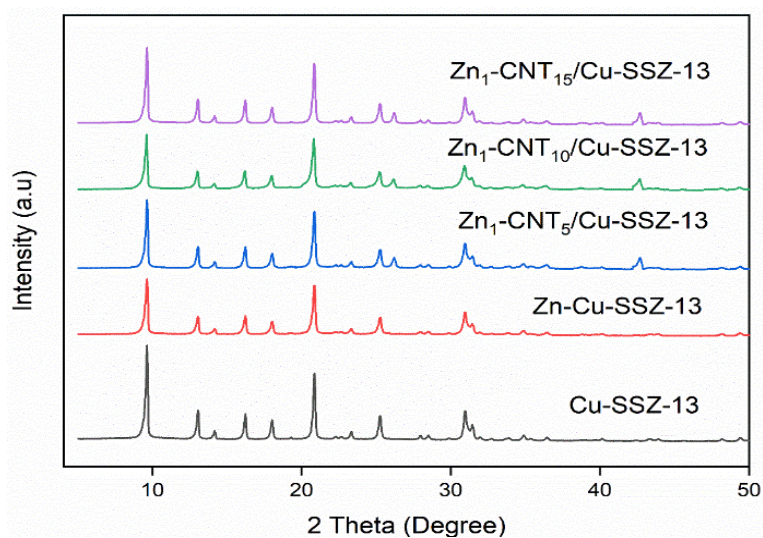


Fig. 2. XRD pattern of Cu-SSZ-13 and hybrid Cu-SSZ-13 zeolite catalyst.

5.1.2 BET Analysis

BET analysis ascribed the surface area of the catalyst with pore volume and pore size. Table 1 exhibits the physical characteristics of Cu-SSZ-13 and hybrid Cu-SSZ-13 zeolite catalyst. From Table 1, it is inferred by the addition of CNTs over Zn/Cu-SSZ-13 zeolite catalyst, the surface area gets increased from 345 m²/g to 500.0681 m²/g. However, the addition of Zn species over Cu-SSZ-13 zeolite catalyst decreases surface area from 389 m²/g to 345 m²/g due to the high dispersion of Zn species over the surface of Cu-SSZ-13 zeolite catalyst, blocking micropores to a small extent. In actuality, H-SSZ-13 has a higher surface area of 656 m²/g for Si/Al ratio of 4.97 [32] and, by the addition of Cu species by ion exchange process, the surface area was reduced to 389 m²/g attributed to the Cu species exchange as cationic with H-SSZ-13 zeolite, blocking few pores stimulated by the higher dispersion on the zeolite surface. The effect of dispersion of Cu, Zn, & CNTs in Cu-SSZ-13 & Zn_x-CNT_y/Cu-SSZ-13 was discussed in catalytic activity.

Table 1. Physical properties of hybrid zeolite catalyst.

S.No	Catalyst	BET Surface Area(m ² /g)	Pore Volume (cm ³ /g)	Pore Size (Å)
1	Cu-SSZ-13	389	0.140353	49.084
2	Zn-Cu-SSZ-13	345	0.11563	49.516
3	Zn ₁ -CNT ₅ /Cu-SSZ-13	362.6523	0.124307	49.277
4	Zn ₁ -CNT ₁₀ /Cu-SSZ-13	428.2102	0.149365	48.693
5	Zn ₁ -CNT ₁₅ /Cu-SSZ-13	500.0681	0.180423	48.229

5.1.3 SEM Analysis

The microscopic structure of Cu-SSZ-13 & hybrid Cu-SSZ-13 zeolite catalyst was shown in Fig.3 in which (a) exhibits the uniform dispersion of Cu species, (b) shows the dispersion of Cu, & Zn, and (c) – (e) shows the dispersion of Cu, Zn, & CNTs in hybrid Zn_x-CNT_y/Cu-SSZ-13 catalyst. The dispersion and elemental composition was further confined by the EDS spectral of CNTs, Cu, & Zn species Fig.4 and Table 2. Further, it is evident from fig.2, that all the species are homogeneously dispersed over the surface of zeolite catalyst and Zn & CNTs species support Cu species in catalytic activity to increase the performance of SCR activity at a wide temperature region.

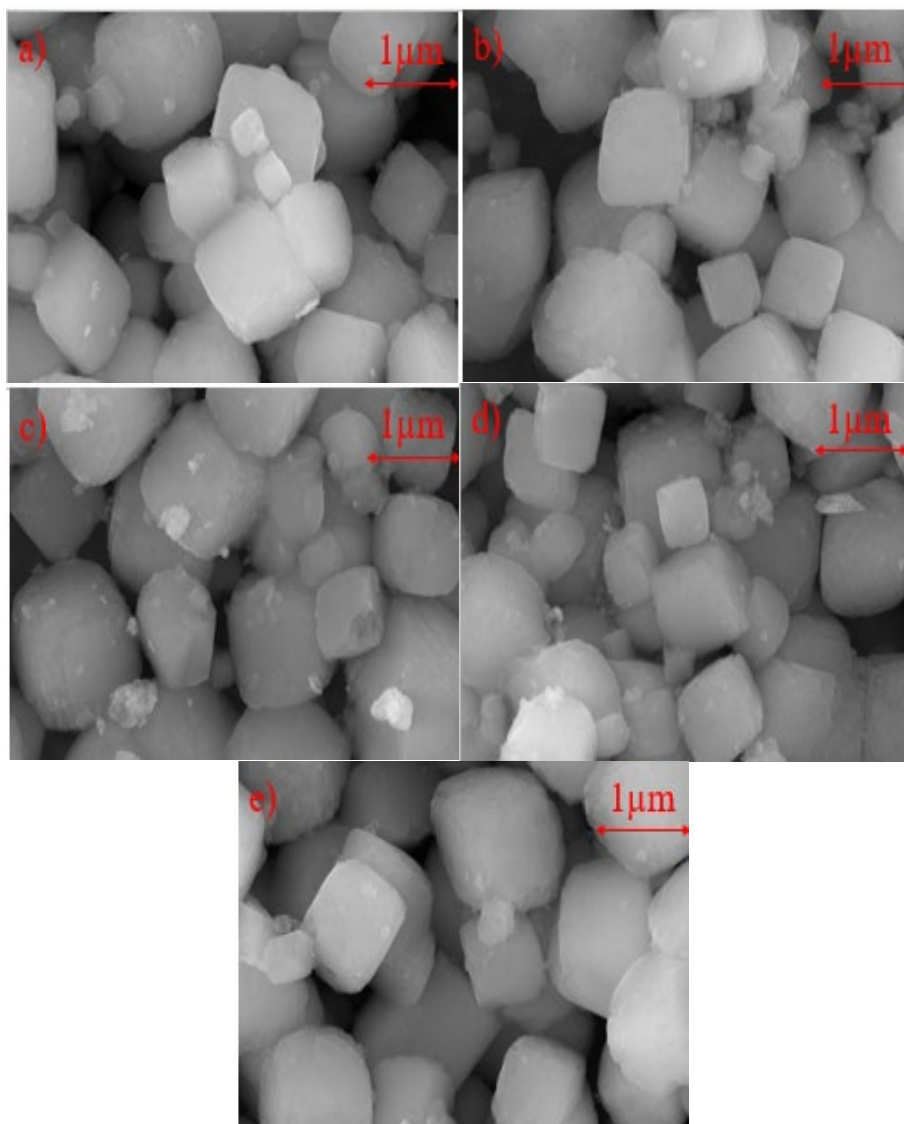


Fig. 3. SEM images of Cu-SSZ-13 and hybrid Cu-SSZ-13 zeolite catalyst.

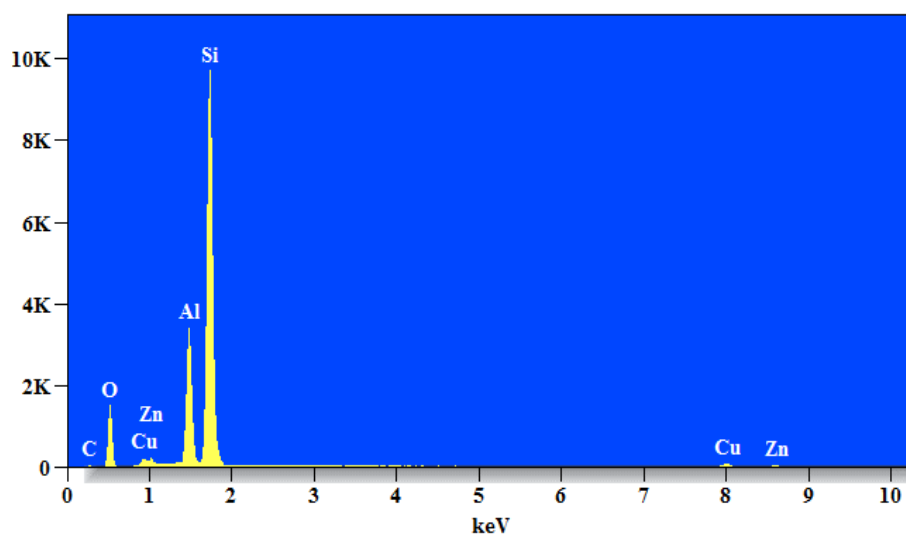


Fig. 4. EDS spectrum of $Zn_x-CNT_y/Cu-SSZ-13$.

Table 2. Elemental composition of catalyst.

Catalyst	Cu (Wt. %)	Zn (Wt. %)	CNT (Wt. %)
Cu-SSZ-13	3.05	-	-
Zn/Cu-SSZ-13	1.93	4.16	-
Zn ₁ -CNT ₅ /Cu-SSZ-13	1.61	1.77	5.15
Zn ₁ -CNT ₁₀ /Cu-SSZ-13	2.95	2.37	2.74
Zn ₁ -CNT ₁₅ /Cu-SSZ-13	1.91	2.46	2.69

5.1.4 XPS Analysis

The copper species of zeolite catalyst was characterized by XPS to define its nature and catalyst composition shown in fig.5. The XPS spectrum of Cu-SSZ-13 and hybrid Cu-SSZ-13 catalysts shown in fig.5 (a) & (b) respectively has two peak intensities corresponding to Cu²⁺ and Cu⁺ in terms of Cu2p_{3/2} and Cu2p_{1/2}, with binding energies of 932.5 eV and 952.3 eV for Cu2p_{3/2} and Cu2p_{1/2} of Cu⁺ species and 933.7 eV and 953.6 eV for Cu2p_{3/2} and Cu2p_{1/2} of Cu²⁺ species, respectively [32]. These species of copper Cu²⁺ and Cu⁺ help the NH₃-SCR activity to take place. By the Zn and CNTs doping on Cu-SSZ-13, the zeolite intensity gets reduced and slightly shifted towards higher binding energy (approximately 0.2 eV), and a broadening effect was evident. Even though, Cu²⁺ species of copper were well-coordinated within the structure of zeolites the broadened peak states to increase in chemisorbed oxygen aid in an increase in NH₃-SCR activity.

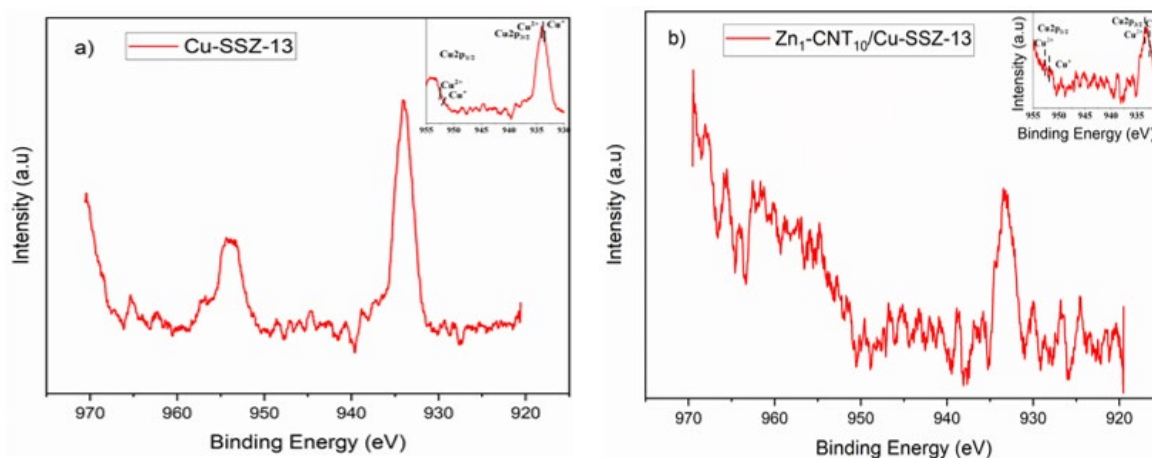


Fig. 5. XPS spectrum of Cu-SSZ-13 and hybrid Cu-SSZ-13 catalysts.

5.1.5 NH₃-TPD

Temperature programmed desorption was carried out to examine the desorption, surface reaction, and adsorption of the catalyst by evaluating the active sites on the surfaces of the catalyst. NH₃-TPD was carried out to examine the active sites of the catalyst surface and their strength [27]. The profiles of NH₃-TPD for Cu-SSZ-13, Zn/Cu-SSZ-13, and Zn-CNT/Cu-SSZ-13 are shown in fig.6. According to the profile of Cu-SSZ-13, low-temperature peak profiles under 186°C, 161°C, and 167°C represent adsorption of NH₃ species on a weaker side indicating physisorbed NH₃ i.e. weaker Lewis acid site [33]–[35] and relates with hydroxyl groups on the surface of catalyst [36]. Temperature peak of middle range in profile leads to copper ion incorporation in CHA structure [37]. As the amount of copper ion changes with the loading of copper over CHA structure and higher peak profile represents Brønsted acid site over 500°C attributes adsorption of NH₃ species.

Due to the addition of Zn in Cu-SSZ-13, the temperature peak at 524°C is attributed to the adsorption of NH₃ species, representing a strong Brønsted acid site specifying a higher capacity of NH₃ adsorption. Increasing weak acid sites by the addition of CNT increases the BET surface area providing ample hydroxyl groups and surface sites for performance of NH₃-SCR by adsorption of NH₃. Even though Cu-SSZ-13 and Zn/Cu-SSZ-13 has similar NH₃ adsorption and surface area at

lower temperature region (167°C & 245°C). Zn-CNT/ Cu-SSZ-13 exhibits a more stable structure than Zn/Cu-SSZ-13 and Cu-SSZ-13 for adsorption of NH₃ at weak sites, with middle-range incorporated with copper ions for peak adsorption at 381°C and peak at 552°C, represents a stronger acid site in Brønsted acid site. It shall be inferred that physisorbed and chemisorbed NH₃ represent desorption at temperature peaks of low and high respectively [38]. The position and area of the desorption peak represent acid strength and amount. From the temperature profile, peaks at low temperature implies strong acid strength, and high temperature implies acid amount, favorable for the oxidation of NH₃ over Zn-CNT/Cu-SSZ-13, besides increased strong acid site and strength [39].

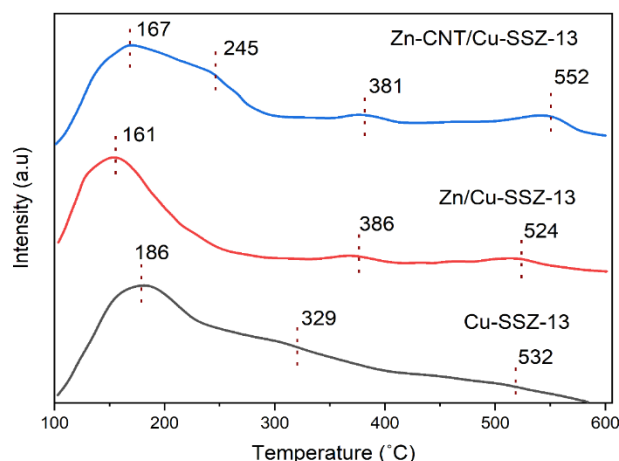


Fig. 6. NH₃-TPD profile of Cu-SSZ-13 and hybrid Cu-SSZ-13 zeolite catalyst.

5.1.6 SO₂-TPD

The catalyst ability for SO₂ adsorption was conducted by SO₂-TPD shown in fig.7. The peaks at 126°C and 146°C represent physisorbed SO₂ [33] whereas higher temperature peaks attribute to copper sulfate decomposition at various sites [14], [22] High intense temperature peaks corresponding to copper sulfate decomposition are observed indicating the formation of copper sulfate by SO₂. At 752°C, a strong peak was identified which indicates copper sulfate decomposition [14], [40], and another high-temperature peak i.e. 832°C was observed in Zn & Zn-CNT based Cu-SSZ-13 hybrid catalyst indicating ZnSO₄ species decomposition [41] and SO₂-TPD profile indicates the decomposition of ZnSO₄& CuSO₄. Rather, the hybrid catalyst has a high tendency to decompose ZnSO₄ than CuSO₄ at a high temperature due to the strongest signal toward Zn-CNT hybrid catalyst.

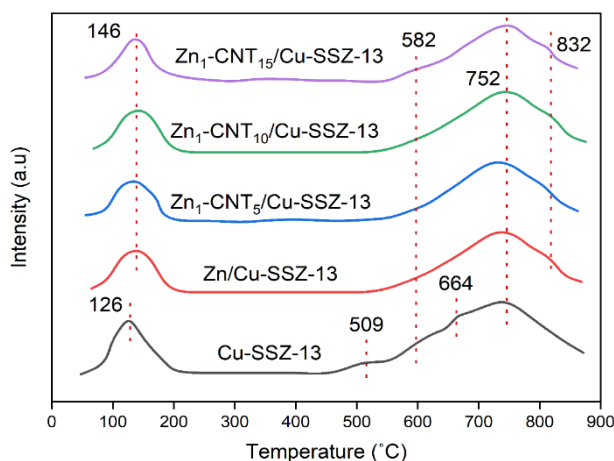


Fig. 7. SO₂-TPD profile of Cu-SSZ-13 and hybrid Cu-SSZ-13 zeolite catalyst.

5.1.7 H₂-TPR

The effect of copper species reducibility was observed by H₂-TPR profile shown in fig. 8. Indicated by the literature, reduction peaks attribute to the reduction of three varieties of copper species namely α , β , & ν . Cu²⁺ as α , CuO as β , and Cu²⁺ as ν are in the structure of CHA & D6R at low temperature (~200°C), middle and high temperature (above 400°C) respectively [37], [42]. Cu-SSZ-13 exhibits peaks at 224°C & 295°C implying 8-MR Cu⁺ ion by reduction of aggregates of CuOx and also peak at 390°C representing 6-MR Cu⁺ by Cu²⁺ reduction [4], [5] whereas, the peak at 564°C represents Cu⁰ by reduction of Cu⁺ [43]. The addition of Zn in Cu-SSZ-13 tends to the decreased H₂ consumption at 217°C, which further increases at 370°C due to the increased concentration of Zn leading to Cu²⁺ migration from 8MR to 6MR. The hybrid catalyst Zn-CNT has three reduction peaks 603°C, 450°C and 210°C leads to Zn-CNT, Zn & surface oxygen species reductions respectively [1], [2], [4], [5], [7], [15]. So, Zn-CNT & Cu-SSZ-13 exhibits strong interaction for reduction of surface copper species.

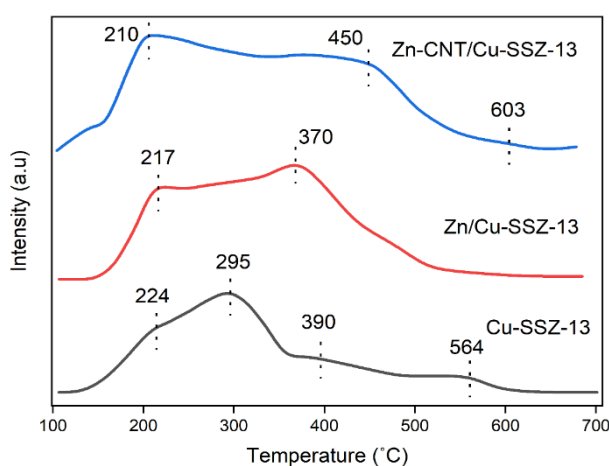


Fig. 8. H₂-TPR profile of Cu-SSZ-13 and hybrid Cu-SSZ-13 zeolite catalyst.

5.2 Catalytic activity

5.2.1 NH₃-SCR activity

Catalytic activity of Cu-SSZ-13 zeolite catalyst and its hybrid zeolite catalyst experimented in NH₃-SCR under gas hourly space velocity of (GHSV) 30,000h⁻¹. Fig.9 shows NOx conversion efficiency of various zeolite hybrid catalyst over Cu-SSZ-13 zeolite catalyst at a reaction condition of 500 ppm NO, 500 ppm NH₃, 6% O₂, & N₂ balance with GHSV of 30,000 h⁻¹. Results indicate that, by the addition of Zn over Cu-SSZ-13 zeolite catalyst, the NOx conversion efficiency slightly gets reduced and upon the addition of CNTs over Zn/Cu-SSZ-13, NOx conversion efficiency increases. In the case of the hybrid Cu-SSZ-13 catalyst, Zn₁-CNT₁₀/Cu-SSZ-13 & Zn₁-CNT₁₅/Cu-SSZ-13 exhibits similar performance rate in lower temperature under which at higher temperature region Zn₁-CNT₁₅/Cu-SSZ-13, NOx conversion gets reduced influenced by the amount of reduction of Cu species and Zn₁-CNT₁₀/Cu-SSZ-13 exhibits better NOx conversion efficiency at the high-temperature window comparatively. The maximum NOx conversion i.e. 100% achieved by each catalyst as follows: Zn₁-CNT₁₀/Cu-SSZ-13 (180°C - 475°C) > Zn₁-CNT₁₅/Cu-SSZ-13 (170°C - 440°C) > Zn₁-CNT₅/Cu-SSZ-13 (240°C - 475°C) > Cu-SSZ-13 (245°C - 375°C) > Zn/Cu-SSZ-13 (250°C - 380°C). Comparatively, Zn₁-CNT₁₅/Cu-SSZ-13 also achieves its maximum NOx conversion at 170°C but exists for a while at higher temperature regime, NOx conversion reduced at 440°C which comparatively lesser applicable towards higher temperature application, whereas Zn₁-CNT₁₀/Cu-SSZ-13 has maximum NOx conversion at 180°C and NOx conversion reduced at almost 475°C but still it maintains NOx conversion higher than 95% at 550°C, so Zn₁-CNT₁₀/Cu-SSZ-13 exhibits better NOx conversion efficiency at both low and higher temperature window best suitable for practical applications due to increased reaction space and time between exhaust emission gas and the catalyst.

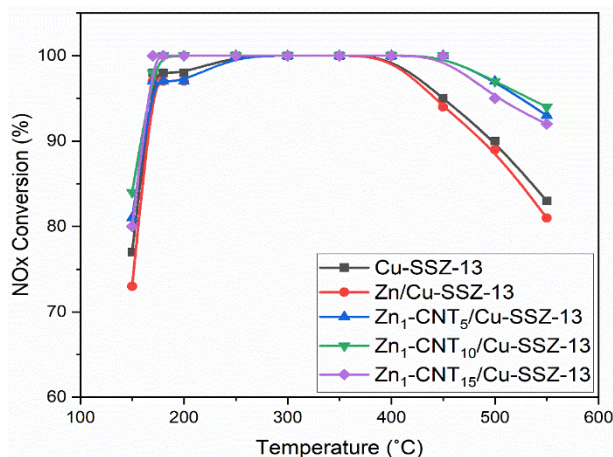


Fig. 9. NOx conversion of hybrid zeolite catalyst over Cu-SSZ-13 zeolite catalyst (Reaction condition 500 ppm NO, 500 ppm NH₃, 6% O₂, & N₂ balance, GHSV: 30,000h⁻¹).

Fig.10 shows NH₃ conversion of hybrid catalyst over Cu-SSZ-13 catalyst under similar conditions. Results indicate that the variation of NH₃ conversion efficiency can be achieved at higher rates only at low temperature window and at high temperature window, NH₃ conversion was not much influenced by hybrid catalyst i.e. all the catalyst has same NH₃ conversion with slight variation region, though the Zn₁-CNT₁₀/ Cu-SSZ-13 has higher rate of NH₃ conversion over typical temperature region. From fig.10 it is implied that the addition of CNTs and Zn species over Cu-SSZ-13 zeolite catalyst doesn't influence in higher rates.

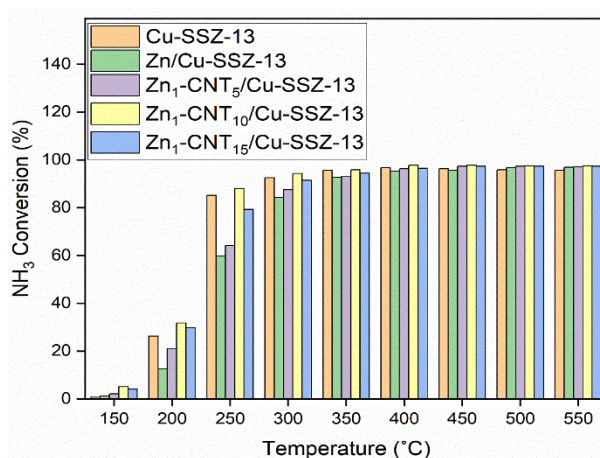


Fig. 10. NH₃ removal efficiency (Reaction condition 500 ppm NO, 500 ppm NH₃, 6% O₂, & N₂ balance, GHSV: 30,000h⁻¹).

5.2.2. Anti-sulfur activity & hydrothermal stability

Sulfur poisoning and hydrothermal stability plays a vital role in reducing the application of NH₃-SCR. In order to reduce it, catalytic activity against SO₂ & H₂O water vapor in feed gas was measured for NOx conversion. Fig.11 exhibits NOx conversion of hybrid catalyst over Cu-SSZ-13 zeolite catalyst with 200 ppm SO₂ & 5% H₂O water vapor in feed gas at 300°C. Anti-sulfur activity & hydrothermal stability was measured for NOx conversion on time-dependent at the same temperature range as almost all catalyst exhibits its maximum NOx conversion without SO₂ & H₂O at 300°C. NOx conversion measurement was carried out for 8hrs at 300°C and the results explain that the NOx conversion efficiency was reduced while SO₂ & H₂O in feed was ON. Among catalyst Cu-SSZ-13 exhibits least NOx conversion of 67%. With the addition of Zn species in Cu-

SSZ-13, NO_x conversion efficiency was increased to 72% because Zn species will attribute to the regeneration ability of active sites of Cu²⁺ & Cu⁺ at 175°C [44]. So, as active sites of Zn-Cu-SSZ-13 are generating gradually, NO_x conversion was achieved by Zn₁-CNT₁₀/Cu-SSZ-13, due to impact of CNTs. Because CNTs increases surface area which regenerates more number of active sites. The NO_x conversion efficiency of catalyst as follows: Zn₁-CNT₁₀/Cu-SSZ-13 (80%) > Zn₁-CNT₅/Cu-SSZ-13 (77%) > Zn₁-CNT₁₅/Cu-SSZ-13 (75%) > Zn/Cu-SSZ-13 (72%) > Cu-SSZ-13 (67%). Once SO₂ & H₂O gas feed was stopped, all the catalyst restores to their original NO_x conversion efficiency with a slight reduction due to the after-effects of SO₂ gas & H₂O water vapor over the surface of active sites and this deactivation is mainly due to elimination of pores, zeolite dealumination and metal sintering [45]. The hybrid zeolite catalyst Zn₁-CNT₁₀/Cu-SSZ-13 exhibits 80% of NO_x conversion in the presence of SO₂ & H₂O in feed gas higher than all catalyst, implies better catalyst towards practical application. It defines the regeneration property of Zn species, influences the NO_x conversion efficiency by regenerating active species and decomposing ZnSO₄, CuSO₄, and resistance towards H₂O.

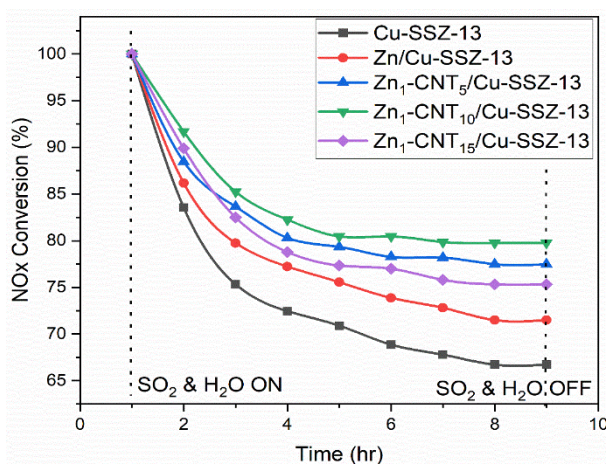


Fig. 11. NO_x conversion of hybrid catalyst over Cu-SSZ-133 catalyst against SO₂ & H₂O in feed gas (Reaction condition 500ppm NO, 500ppm NH₃, 6% O₂, 200ppm SO₂ (while used), 5% H₂O (while used), and balance N₂).

5.3. Discussion

Cu-SSZ-13 chabizite structure zeolite catalyst was prepared by ion exchange method and hybrid Cu-SSZ-13 zeolite catalyst was prepared by wet impregnation method. From BET analysis, it is identified that the surface area of Cu-SSZ-13 was reduced by doping of Zn species but catalytic activity was not negatively influenced shown in Fig.9. With the addition of CNTs over Zn/Cu-SSZ-13 zeolite to various molar ratio in between Zn_x-CNT_y as 1:5, 1:10, & 1:15, the amount of CNTs dispersed on Zn/Cu-SSZ-13 was clearly evident in both EDS & XRD. From Fig.4, it is known that CNTs, & Zn species are well dispersed over Cu-SSZ-13 catalyst and from Fig.2 shows that presence of CNTs by intensities of the peaks (2θ) around 26.4° & 42.5°, which influences on surface area enhancement. As increase in CNTs, BET surface area increased as shown in Table 1. Even though surface area of Zn₁-CNT₁₅/Cu-SSZ-13 has high BET surface area catalytic activity was not affected for Zn₁-CNT₁₀/Cu-SSZ-13, indicating surface area reduction due to Zn species doping will not affect the catalytic activity. From Fig.5, Cu²⁺ & Cu⁺ active sites are found over 933.7 eV & 953.6 eV, and 932.5 eV, & 952.3 eV respectively which acts as active sites for the catalytic activity. Doping of Zn & CNTs increases the intensities of Cu²⁺ and Cu⁺ peaks get reduced further compensated by the increase in the surface area and Zn species which regenerates active sites at 175°C itself. So, these phenomenal change enhances the performance of NH₃-SCR. Figures 6, 7, & 8, indicate that hybrid catalyst Zn_x-CNT_y/Cu-SSZ-13 has the strongest acidity and redox activity i.e. provides more active sites for Cu²⁺ and Cu⁺ with low oxidation of Cu species aid in activity enhancement of NH₃-SCR.

6. Conclusion

Cu-SSZ-13 zeolite catalyst and a series of hybrid Cu-SSZ-13 zeolite catalysts with the different molar ratios of Zn_x : CNT_y as 1:5, 1:10, & 1:15 with the mass ratio of 1:5 between Zn_x : CNT_y/Cu-SSZ-13 was successfully synthesized by ion-exchange and wet-impregnation method. From the characterization of Cu-SSZ-13 catalyst and hybrid Cu-SSZ-13 catalyst by BET, XRD XPS, NH₃-TPD, SO₂-TPD, & H₂-TPR it shall be concluded that both Zn & CNTs species were well dispersed over Cu-SSZ-13 species which CNTs increases the surface area of the catalyst and Zn regenerates active sites of Cu²⁺ & Cu⁺ and concluded with the low oxidation state of Cu species enhancing the activity of NH₃-SCR.

Catalytic activity examination results conclude that the hybrid Zn₁-CNT₁₀/Cu-SSZ-13 zeolite catalyst exhibits maximum NO_x conversion i.e. 100% at 180°C- 475°C finding them suitable for both low and high-temperature application and anti-sulfur NO_x conversion achieved to 80% at 300°C when 200 ppm of SO₂ gas was feed and it restores its initial condition with slight reduction once SO₂ gas in feed was OFF.

Abbreviations

BET	Brunauer-Emmett-Teller	TPD	Temperature Programmed Desorption
GHSV	Gas Hourly Space Velocity	TPR	Temperature Programmed reduction
NH ₃ -SCR	Ammonia Selective Catalytic Reduction	XRD	X-ray Diffraction
SEM	Scanning Electron Microscope	XPS	X-ray Photoelectron Spectroscopy

References

- [1] R. Zhang, N. Liu, Z. Lei, B. Chen, Chemical Reviews 116(6), 3658-3721 (2016); <https://doi.org/10.1021/acs.chemrev.5b00474>
- [2] J. Li, H. Chang, L. Ma, J. Hao, R. T. Yang, Catalysis Today 175(1), 147-156 (2011); <https://doi.org/10.1016/j.cattod.2011.03.034>
- [3] L. Chen et al, Fuel 320, 123969 (2022); <https://doi.org/10.1016/j.fuel.2022.123969>
- [4] Z. Zhao et al, Applied Catalysis B Environmental 217, 421-428 (2017); <https://doi.org/10.1016/j.apcatb.2017.06.013>
- [5] Z. Zhao et al, Catalysis Science and Technology 9(1), 241-251 (2019).
- [6] Y. Jangjou, D. Wang, A. Kumar, J. Li, W. S. Epling, ACS Catalysis 6(10), 6612-6622 (2016); <https://doi.org/10.1021/acscatal.6b01656>
- [7] L. Olsson et al, Applied Catalysis B Environmental 183, 394-406 (2016); <https://doi.org/10.1016/j.apcatb.2015.11.001>
- [8] K. Wijayanti et al, Catalysis Science and Technology 6(8), 2565-2579 (2016); <https://doi.org/10.1039/C5CY01288K>
- [9] W. Su, Z. Li, Y. Zhang, C. Meng, J. Li, Catalysis Science and Technology 7(7), 1523-1528 (2017); <https://doi.org/10.1039/C7CY00302A>
- [11] P. S. Hammershøi, Y. Jangjou, W. S. Epling, A. D. Jensen, T. V. W. Janssens, Applied Catalysis B Environmental 226, 38-45 (2018); <https://doi.org/10.1016/j.apcatb.2017.12.018>
- [12] P. S. Hammershøi, A. D. Jensen, T. V. W. Janssens, Applied Catalysis B Environmental 238, 104-110 (2018); <https://doi.org/10.1016/j.apcatb.2018.06.039>
- [13] K. Wijayanti, K. Xie, A. Kumar, K. Kamasamudram, L. Olsson, Applied Catalysis B Environmental 219, 142-154 (2017); <https://doi.org/10.1016/j.apcatb.2017.07.017>
- [14] Y. Jangjou et al, ACS Catalysis 8(2), 1325-1337 (2018); <https://doi.org/10.1021/acscatal.7b03095>
- [15] J. Chen, R. Zhao, R. Zhou, ChemCatChem 10(22), 5182-5189 (2018); <https://doi.org/10.1002/cctc.201801234>

- [16] T. Gu, R. Jin, Y. Liu, H. Liu, X. Weng, Z. Wu, *Applied Catalysis B Environmental* 129, 30-38 (2013); <https://doi.org/10.1016/j.apcatb.2012.09.003>
- [17] S. S. R. Putluru, L. Schill, A. D. Jensen, B. Siret, F. Tabaries, R. Fehrmann, *Applied Catalysis B Environmental* 165, 628-635 (2015); <https://doi.org/10.1016/j.apcatb.2014.10.060>
- [18] P. S. Hammershøi, P. N. R. Vennestrøm, H. Falsig, A. D. Jensen, T. V. W. Janssens, *Applied Catalysis B Environmental* 236, 377-383 (2018); <https://doi.org/10.1016/j.apcatb.2018.05.038>
- [19] S. Yang et al, *Applied Catalysis B Environmental* 181, 570-580 (2016); <https://doi.org/10.1016/j.apcatb.2015.08.023>
- [20] L. J. France et al, *Applied Catalysis B Environmental* 206, 203-215 (2017); <https://doi.org/10.1016/j.apcatb.2017.01.019>
- [21] S. Raja, M. S. Alphin, L. Sivachandiran, P. Singh, D. Damma, *Fuel* 307, 121886 (2022); <https://doi.org/10.1016/j.fuel.2021.121886>
- [22] Y. Jangjou et al, *Catalysis Science and Technology* 6(8), 2679-2685 (2016); <https://doi.org/10.1039/C5CY02212F>
- [23] S. Bai, Z. Wang, H. Li, X. Xu, M. Liu, *Fuel* 194, 36-41 (2017); <https://doi.org/10.1016/j.fuel.2016.12.074>
- [24] P. Shi et al, *Fuel* 318, 123633 (2022); <https://doi.org/10.1016/j.fuel.2022.123633>
- [25] M. Shen, Y. Zhang, J. Wang, C. Wang, J. Wang, *Journal of Catalysis* 358, 277-286 (2018); <https://doi.org/10.1016/j.jcat.2017.12.008>
- [26] S. Raja, M. S. Alphin, *Journal of Nanoparticle Research* 22(7), 190 (2020); <https://doi.org/10.1007/s11051-020-04919-2>
- [27] S. Raja, M. S. Alphin, *Reaction Kinetics, Mechanics and Catalysis* 129(2), 787-804 (2020); <https://doi.org/10.1007/s11144-020-01735-6>
- [28] T. Zhang et al, *AIChE Journal* 61(11), 3825-3837 (2015); <https://doi.org/10.1002/aic.14923>
- [29] J. Wang, Z. Peng, Y. Chen, W. Bao, L. Chang, G. Feng, *Chemical Engineering Journal* 263, 9-19 (2015); <https://doi.org/10.1016/j.cej.2014.10.086>
- [30] R. H. Athab, B. H. Hussein, *Digest Journal of Nanomaterials and Biostructures* 17(4), 1173-1180 (2022); <https://doi.org/10.15251/DJNB.2022.173.1173>
- [31] S. A. Najim, M. M. Alyas, A. A. Sulaiman, *Digest Journal of Nanomaterials and Biostructures* 17(2), 677-683 (2022); <https://doi.org/10.15251/DJNB.2022.172.677>
- [32] H. Wang, R. Xu, Y. Jin, R. Zhang, *Catalysis Today* 327, 295-307 (2019); <https://doi.org/10.1016/j.cattod.2018.04.035>
- [33] D. Wang, F. Gao, C. H. F. Peden, J. Li, K. Kamasamudram, W. S. Epling, *ChemCatChem* 6(6), 1579-1583 (2014); <https://doi.org/10.1002/cctc.201402010>
- [34] Y. J. Kim, J. K. Lee, K. M. Min, S. B. Hong, I.-S. Nam, B. K. Cho, *Journal of Catalysis* 311, 447-457 (2014); <https://doi.org/10.1016/j.jcat.2013.12.012>
- [35] F. Gao et al *Materials Letters* 138, 25-28 (2015); <https://doi.org/10.1016/j.matlet.2014.09.088>
- [36] J. Wang et al, *Journal of Catalysis* 322, 84-90 (2015); <https://doi.org/10.1016/j.jcat.2014.11.010>
- [37] D. J. Kim, J. Wang, M. Crocker, *Catalysis Today* 231, 83-89 (2014); <https://doi.org/10.1016/j.cattod.2013.10.061>
- [38] B. Guan, H. Lin, L. Zhu, Z. Huang, *Journal of Physical Chemistry* 115(26), 12850-12863 (2011); <https://doi.org/10.1021/jp112283g>
- [39] W. Tian, H. Yang, X. Fan, X. Zhang, *Journal of Hazardous Materials* 188(1), 105-109 (2011); <https://doi.org/10.1016/j.jhazmat.2011.01.078>
- [40] A. M. Gadalla, *International Journal of Chemical Kinetics* 16(6), 655-668 (1984); <https://doi.org/10.1002/kin.550160604>
- [41] J. Straszko, M. Olszak-Humienik, J. Mozejko, *Thermochimica Acta* 292(1), 145-150 (1997); [https://doi.org/10.1016/S0040-6031\(96\)03114-0](https://doi.org/10.1016/S0040-6031(96)03114-0)
- [42] J. Xue, X. Wang, G. Qi, J. Wang, M. Shen, W. Li, *Journal of Catalysis* 297, 56-64 (2013); <https://doi.org/10.1016/j.jcat.2012.09.020>

- [43] L. Xie, F. Liu, L. Ren, X. Shi, F.-S. Xiao, H. He, *Environmental Science and Technology* 48(1), 566-572 (2014); <https://doi.org/10.1021/es4032002>
- [44] R. Yu, Z. Zhao, S. Huang, W. Zhang, *Applied Catalysis B Environmental* 269, 118825 (2020); <https://doi.org/10.1016/j.apcatb.2020.118825>
- [45] C. H. Bartholomew, *Applied Catalysis A: General* 212(1), 17-60 (2001); [https://doi.org/10.1016/S0926-860X\(00\)00843-7](https://doi.org/10.1016/S0926-860X(00)00843-7)